Earth's Future

Supporting Information for

Carbon cycle response to temperature overshoot beyond 2 °C – an analysis of CMIP6 models

I. Melnikova[1,2], O. Boucher[1], P. Cadule[1], P. Ciais[3], T. Gasser[4], Y. Quilcaille[4], H. Shiogama[2], K. Tachiiri[2,5], T. Yokohata[2] and K. Tanaka[2,3]

[1] Institut Pierre-Simon Laplace, Sorbonne Université / CNRS, France

[2] Center for Global Environmental Research (CGER), National Institute for Environmental Studies (NIES), Japan

[3] Laboratoire des Sciences du Climat et de l'Environnement (LSCE), Commissariat à l'énergie atomique et aux énergies alternatives (CEA CNRS UVSQ), Gif-sur-Yvette, France

[4] International Institute for Applied Systems Analysis (IIASA), Austria

[5] Research Institute for Global Change, Japan Agency for Marine-Earth Science and Technology, Japan

Contents of this file

Introduction

This supporting information contains a table and fifteen figures.

Table S1. Ensemble members used in each experiment and each model

ESM	IPSL-CM6A-LR	CNRM-ESM2-1	CanESM5	MIROC-ES2L	UKESM1-0-LL	CESM2-WACCM
piControl	r1i1p1f1	r1i1p1f2	r1i1p1f1, r1i1p2f1	r1i1p1f2	r1i1p1f2 (parent to r4..)	r1i1p1f1
historical	r1i1p1f1 (1910)	r1i1p1f2 (1850)	r1i1p1f1 (5201)	r1i1p1f2 (1850)	r4i1p1f2 (1960)	r1i1p1f1 (55)
ssp534-over	r1i1p1f1	r1i1p1f2	r1i1p1f1	r1i1p1f2	r4i1p1f2	r1i1p1f1
ssp585	r1i1p1f1	r1i1p1f2	r1i1p1f1	r1i1p1f2	r4i1p1f2	r1i1p1f1
hist-bgc	r1i1p1f1 (1910)	r1i1p1f2 (1850)	r1i1p2f1 (5550)	r1i1p1f2 (1850)	r4i1p1f2 (1960)	
ssp534-over-bgc	r1i1p1f1	r1i1p1f2	r1i1p2f1	r1i1p1f2	r4i1p1f2	
ssp585-bgc	r1i1p1f1	r1i1p1f2	r1i1p2f1	r1i1p1f2	r4i1p1f2	

Values in the bracket indicate the branching year from the piControl.

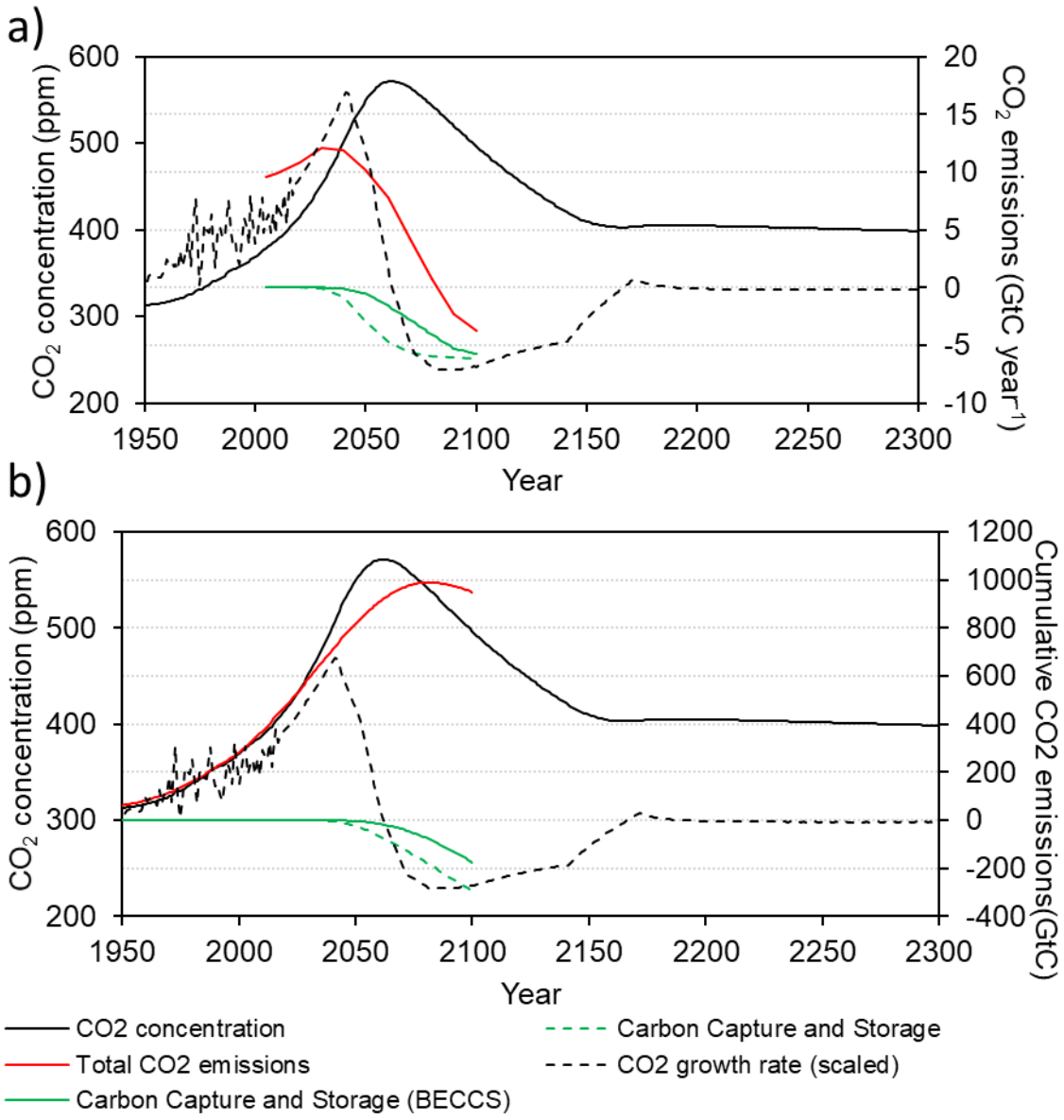

Figure S1. Time series of CO_2 concentration (ppm), CO_2 growth rate (scaled) and corresponding (a) CO_2 emissions (GtC year^{-1}) and (b) cumulative CO_2 emissions (GtC) by REMIND-MAgPIE from input4MIP for SSP-5-3.4-OS experiment. Emission data are from the Integrated Assessment Modeling Consortium & International Institute for Applied Systems Analysis (IIASA) database at https://tntcat.iiasa.ac.at/SspDb/dsd?Action=htmlpage&page=welcome. Fossil fuel emission data prior year 2005 are from the GCB2019 data set.

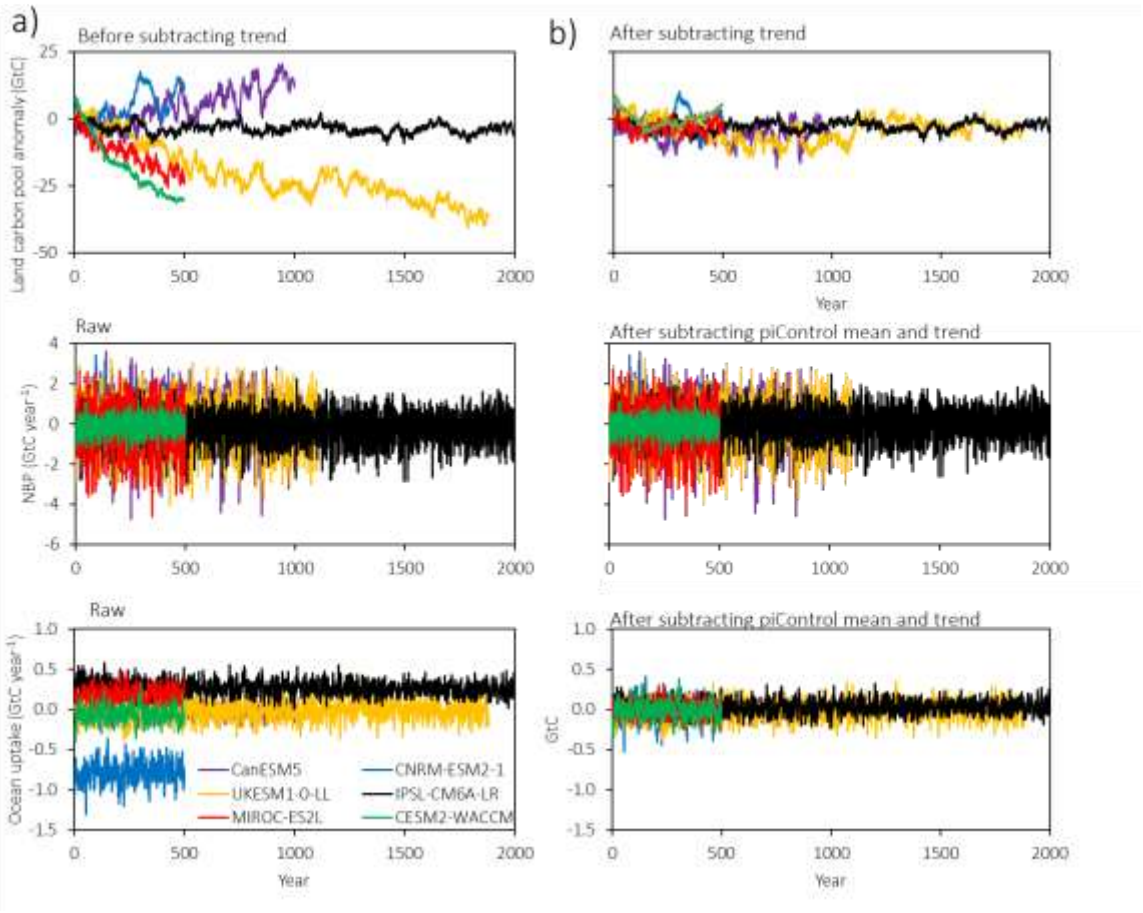

Figure S2. Time series of changes in global land biomass, land (NBP), and ocean carbon uptakes in the piControl experiment before (a) and after (b) pre-processing.

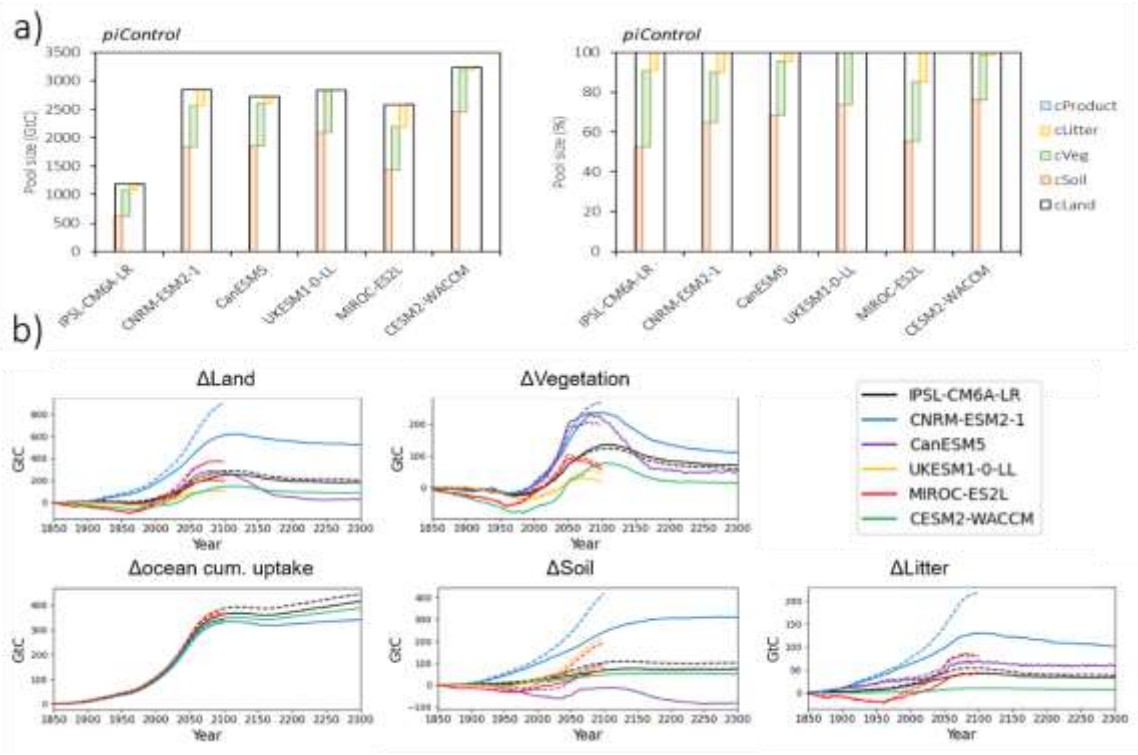

Figure S3. Mean land carbon pool sizes in piControl by six earth system models in fully and biogeochemically coupled simulations of SSP5-3.4-OS experiment (a). Time series of land carbon pools and cumulative ocean flux anomalies from piControl (b). Solid lines indicate COU run, and dashed lines indicate BGC run.

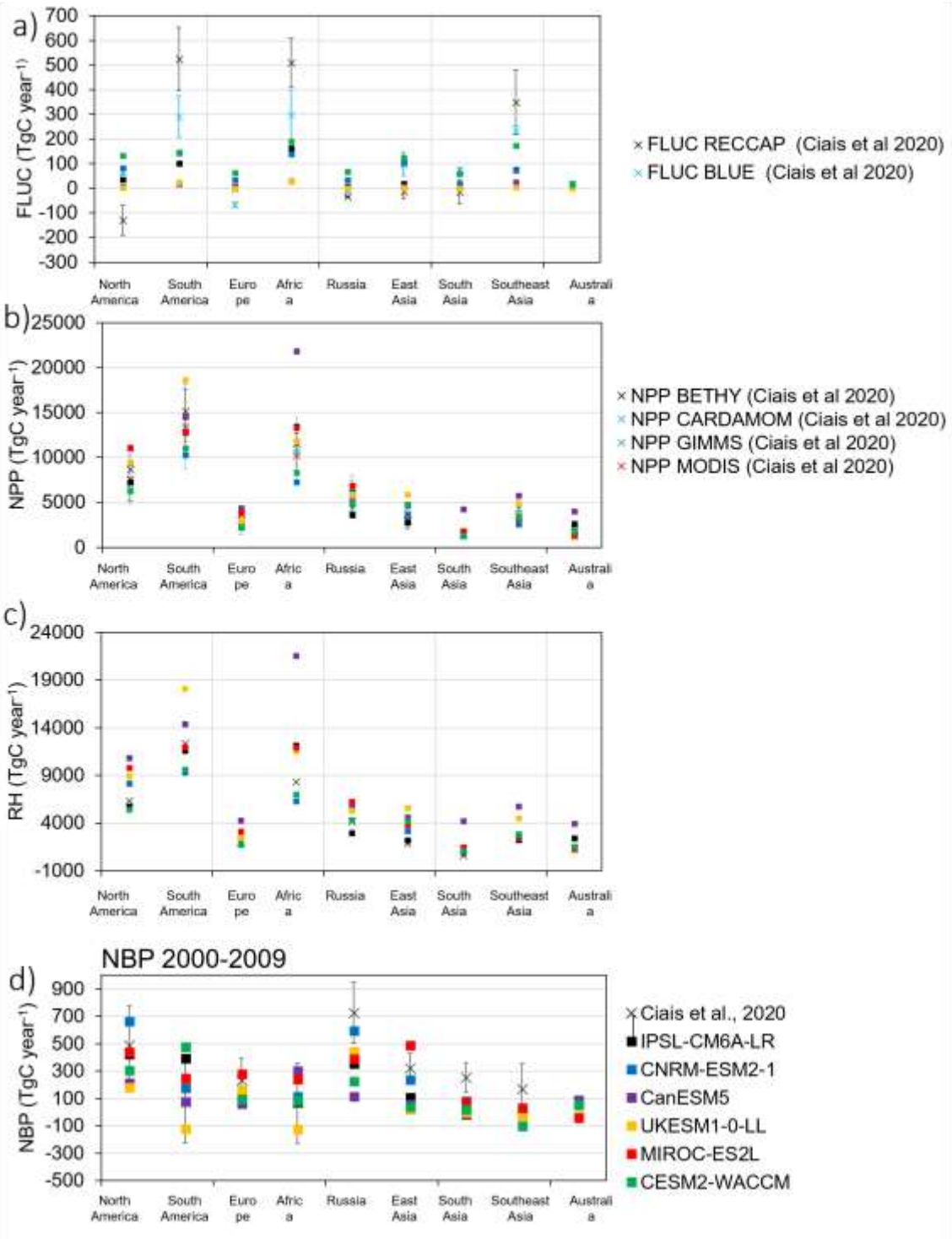

Figure S4. An evaluation of Earth system models (ESMs) against observational data set by Ciais et al. (2020). (a) fLUC, (b) NPP, (c) R_H, and (d) NBP absolute value with associated uncertainty at nine RECCAP regions in 2000-2009.

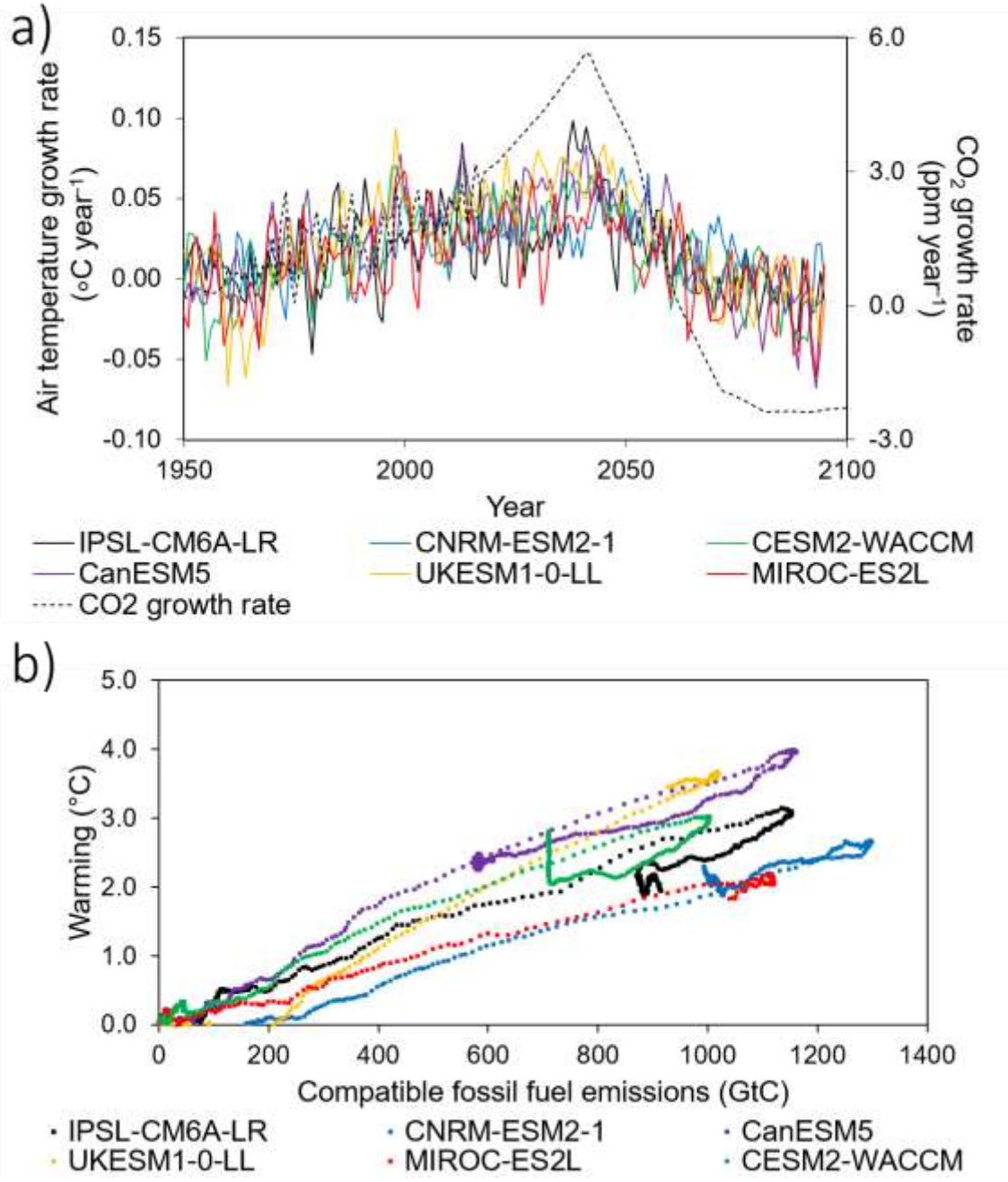

Figure S5. Time series of the growth rate of air temperature and by six earth system models and CO_2 concentration in SSP5-3.4-OS experiment (a). Rates of change in air temperature are given as a 10-year moving average. The surface air temperature changes relative to 1850–1999 mean versus cumulative compatible fossil fuel emissions in the SSP5-3.4-OS pathway (b). The slope of the curves is the transient climate response to cumulative emissions (TCRE).

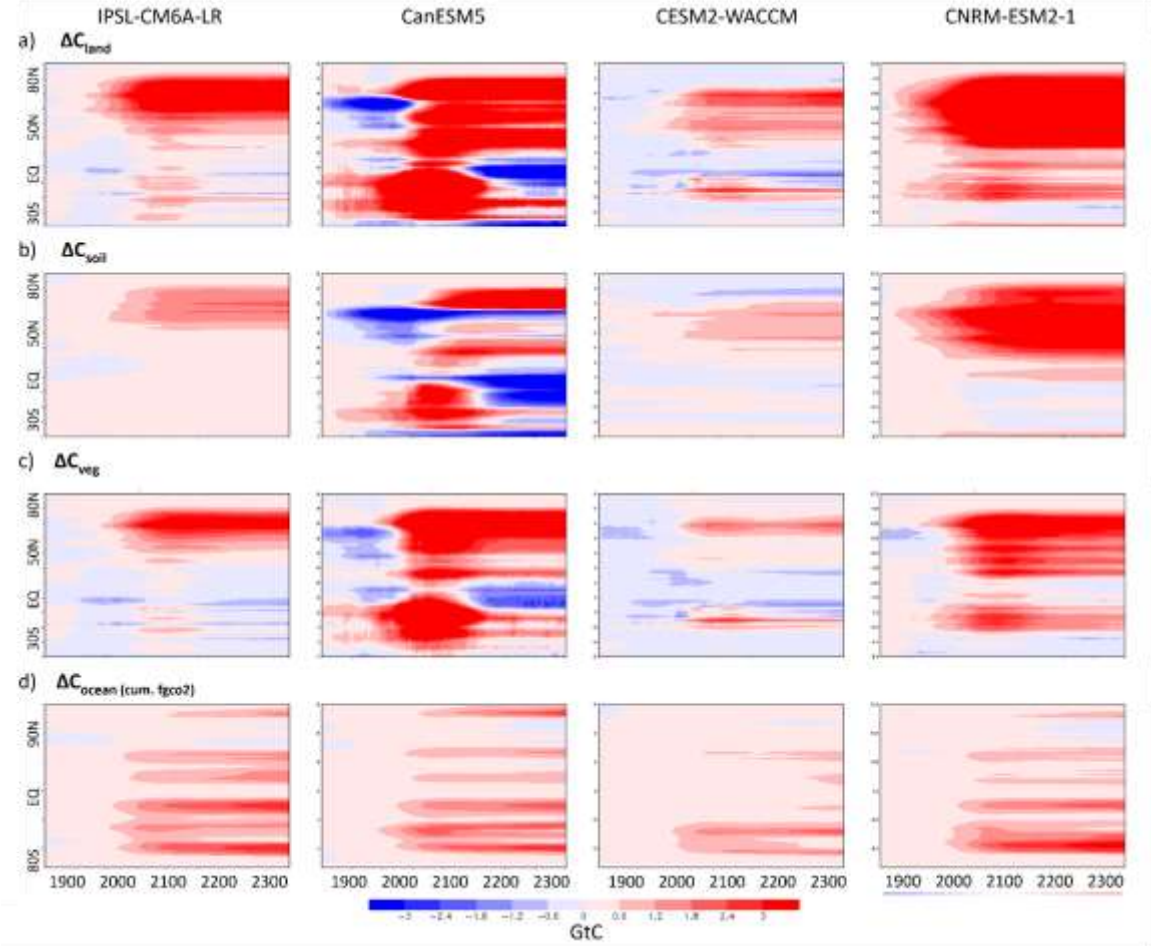

Figure S6. The spatiotemporal variation of zonal cumulative (a) ΔC_{land}, (b) ΔC_{soil}, (c) $\Delta C_{soil,}$ and ΔC_{ocean} (GtC) in 1900-2300 under SSP5-3.4-OS pathway. ΔC_{ocean} is calculated from cumulative flux fgco2 over time.

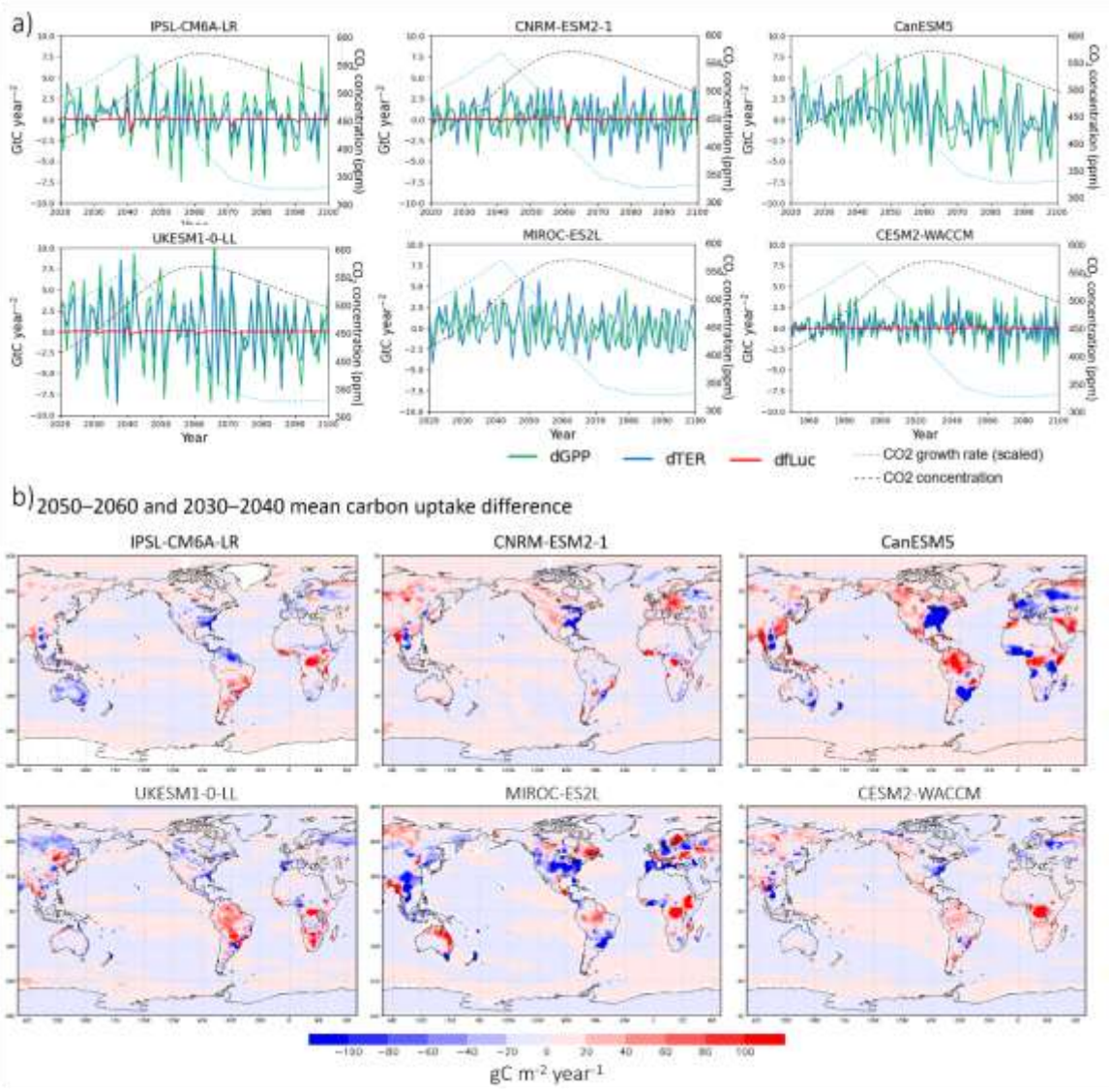

Figure S7. Panel (a) shows the time series of the derivatives of GPP, TER, fLUC (GtC year^{-2}), CO2 concentration (ppm), and scaled CO2 growth rate. fLUC is missing in CanESM5 and MIROC-ES2L because model teams did not provide this variable. Panel (b) shows the spatial variation of the difference between the mean ocean and land uptakes (NBP and fgco2) in 2050–2060 and 2030–2040. Positive values indicate an increase in carbon uptake in a later period.

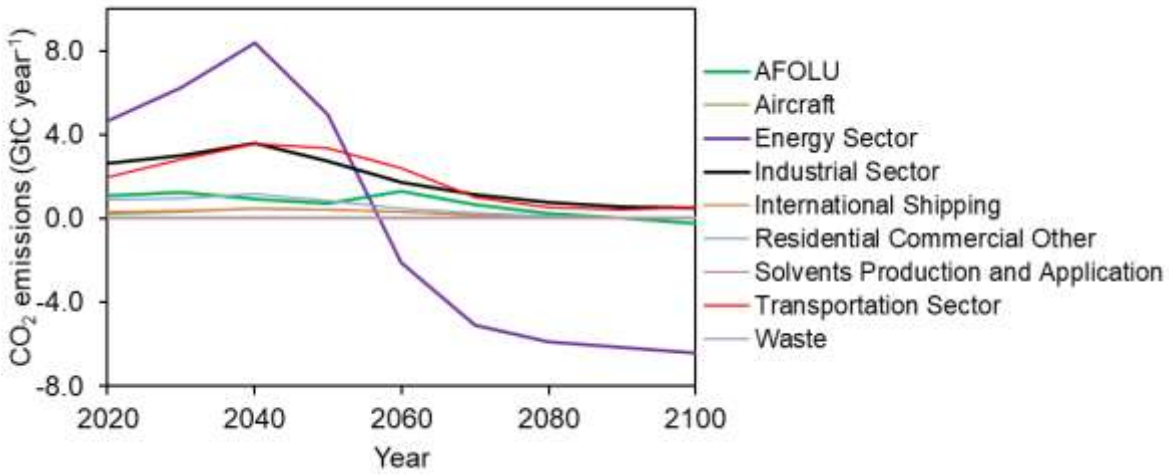

Figure S8. Time series of changes in CO_2 emissions simulated by REMIND-MAGPIE under SSP5-3.4-OS pathway.

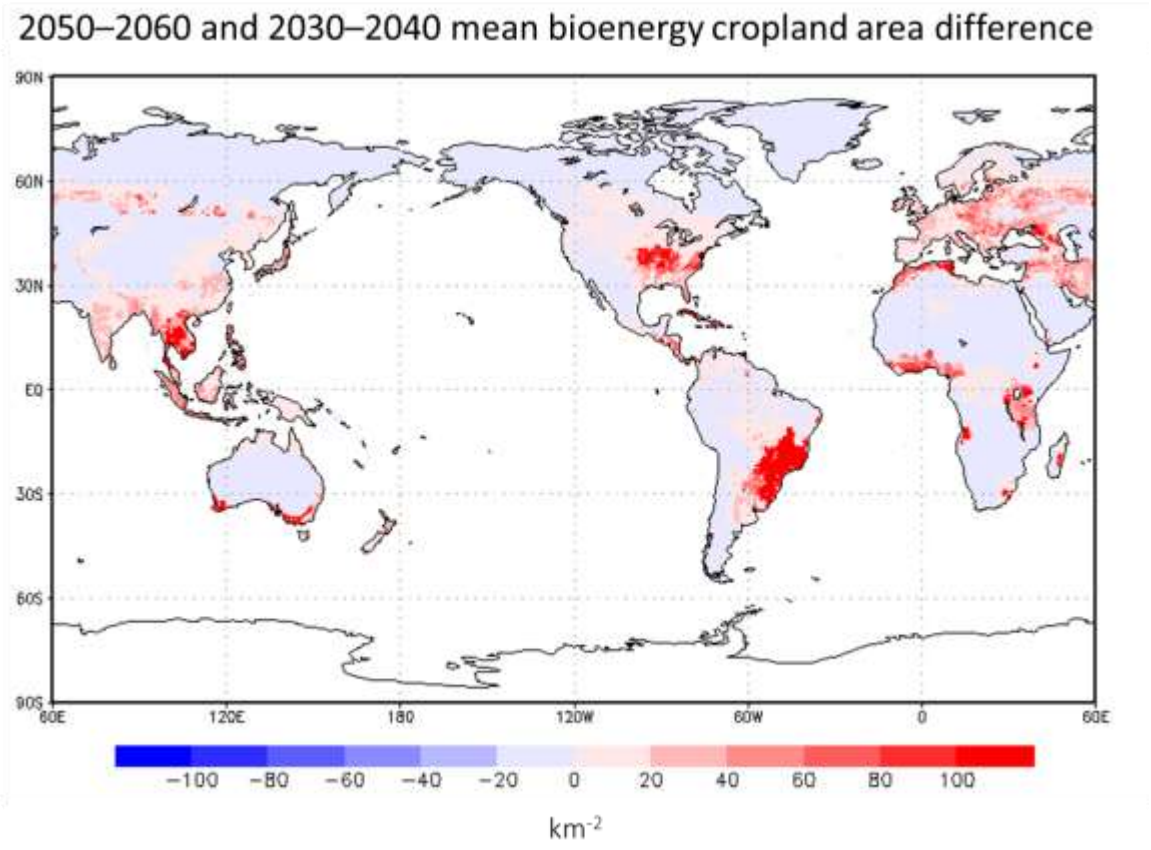

Figure S9. Difference between the mean bioenergy cropland area in 2050–2060 and 2030–2040 based on the LUH2 data set.

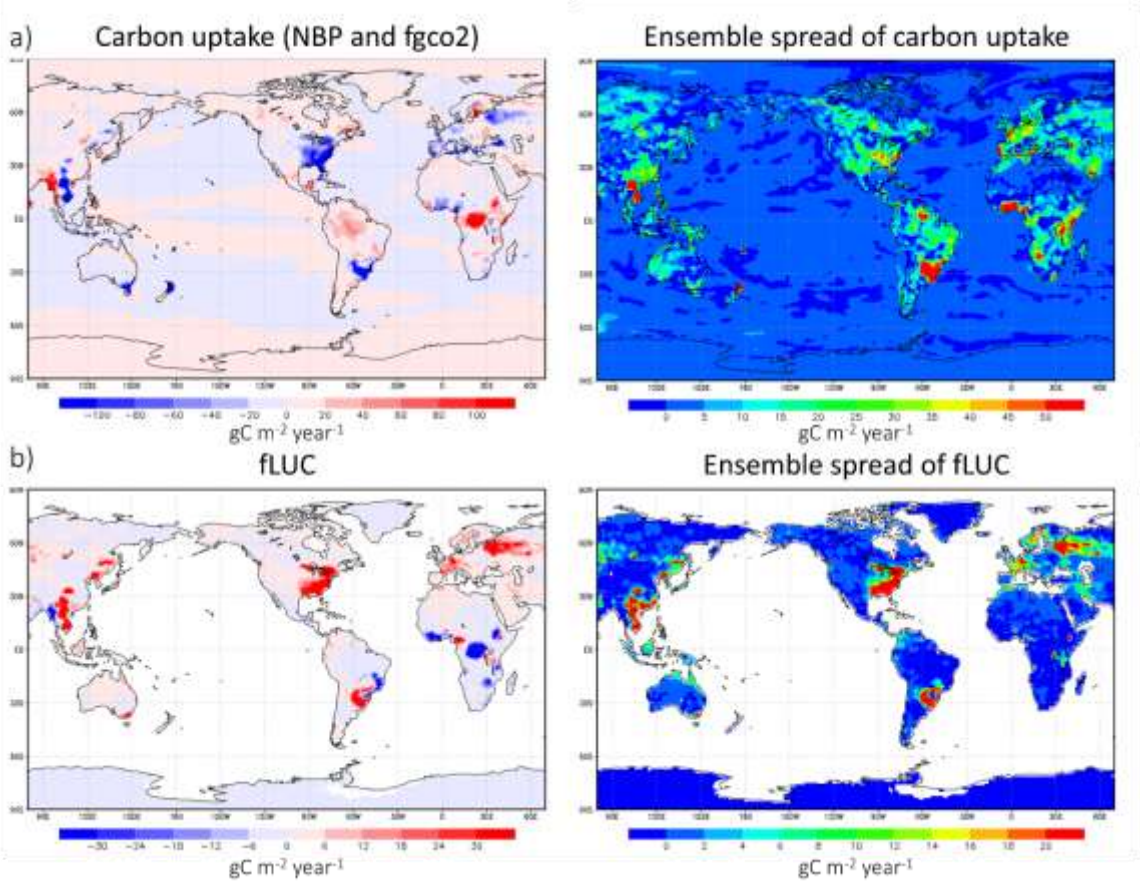

Figure S10. The difference in (a) the carbon uptake and (b) land-use change emissions before and after the peak of CO_2 concentration is shown as ensemble means of six (four for fLUC) CMIP6 ESMs.

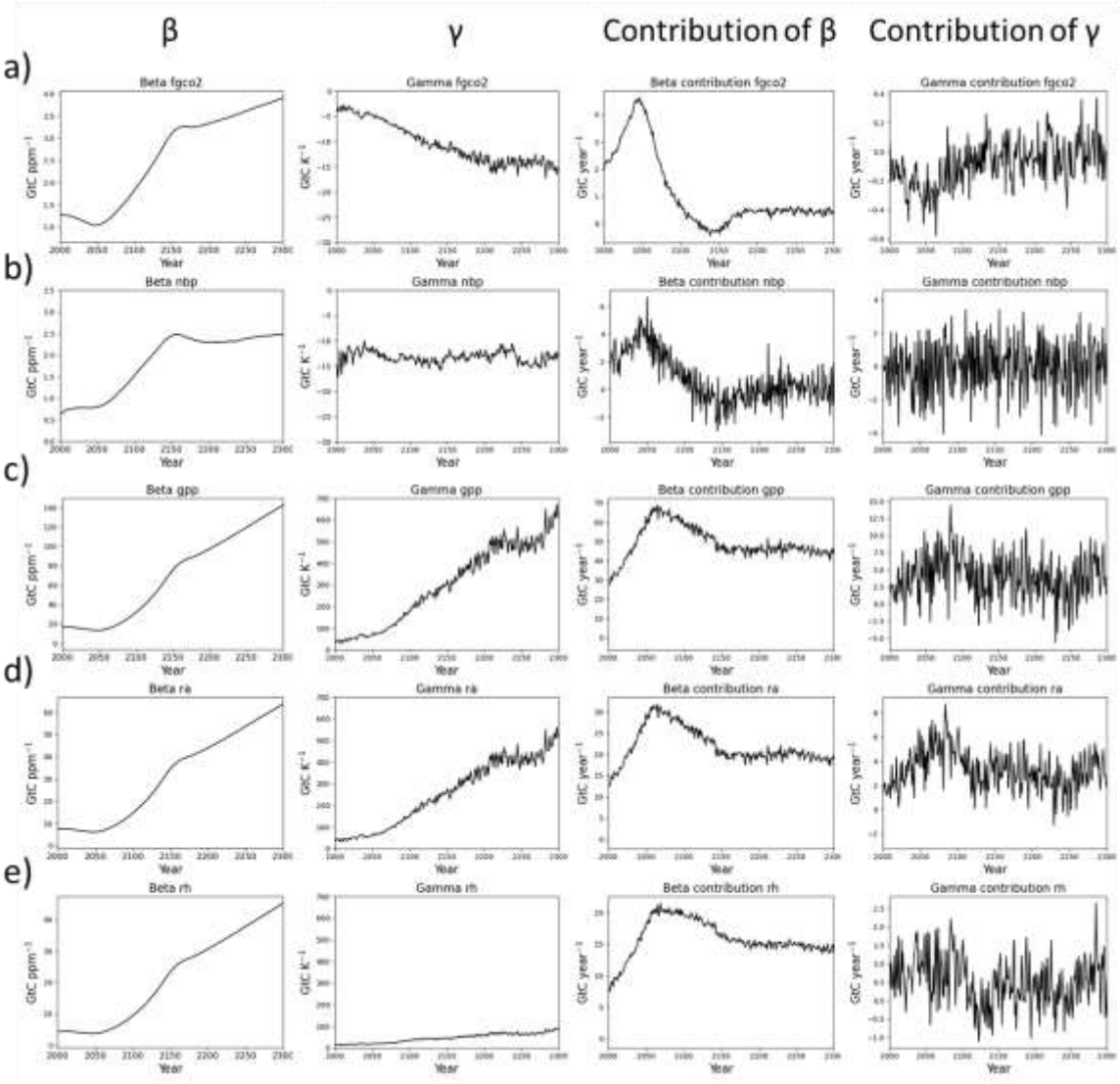

Figure S11. Carbon-concentration β (GtC ppm^{-1}), carbon-temperature γ (GtC $°C^{-1}$) feedback parameters and their contributions to the carbon fluxes (GtC $year^{-1}$) for (a) ocean fgco2, and land (b) NBP, (c) GPP, (d) R_A and (e) R_H as a function of time (year) extended till the year 2300 for IPSL-CM6A-LR under the SSP5-3.4-OS pathway.

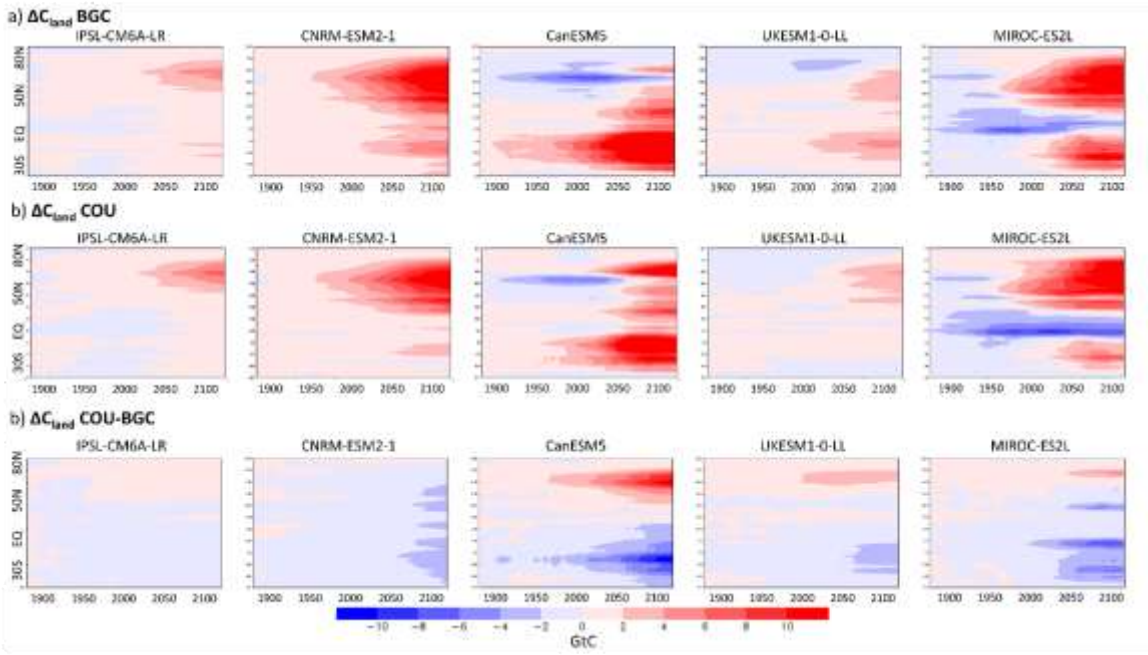

Figure S12. The spatiotemporal variation of zonal cumulative land carbon pool (positive to land) in (a) BGC simulation, (b) COU simulation, and (c) COU-BGC difference.

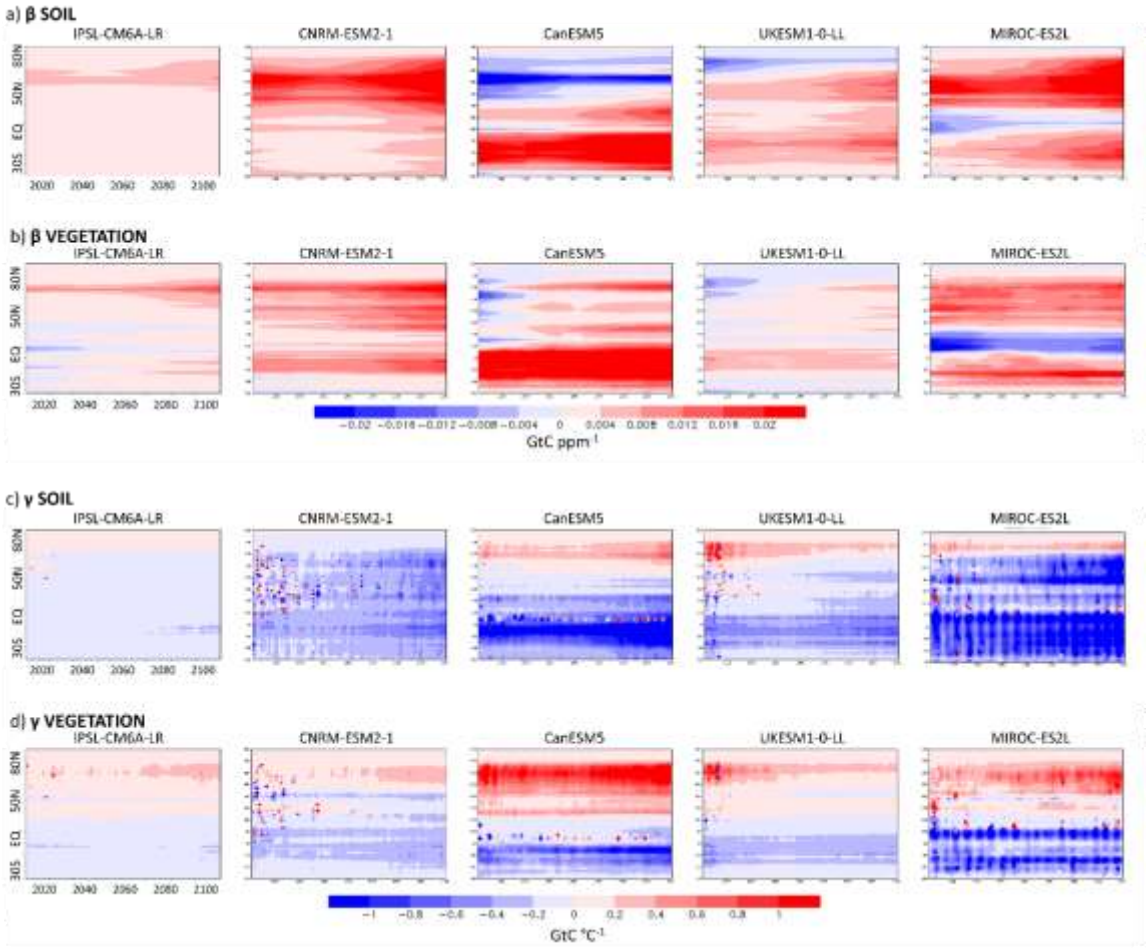

Figure S13. The spatiotemporal variation of zonal cumulative (a) β_{soil}, (b) β_{veg} (GtC ppm-1), (c) γ_{soil} and (d) γ_{veg} (GtC °C^{-1}) calculated from corresponding land carbon pools. Positive values indicate a net sink.

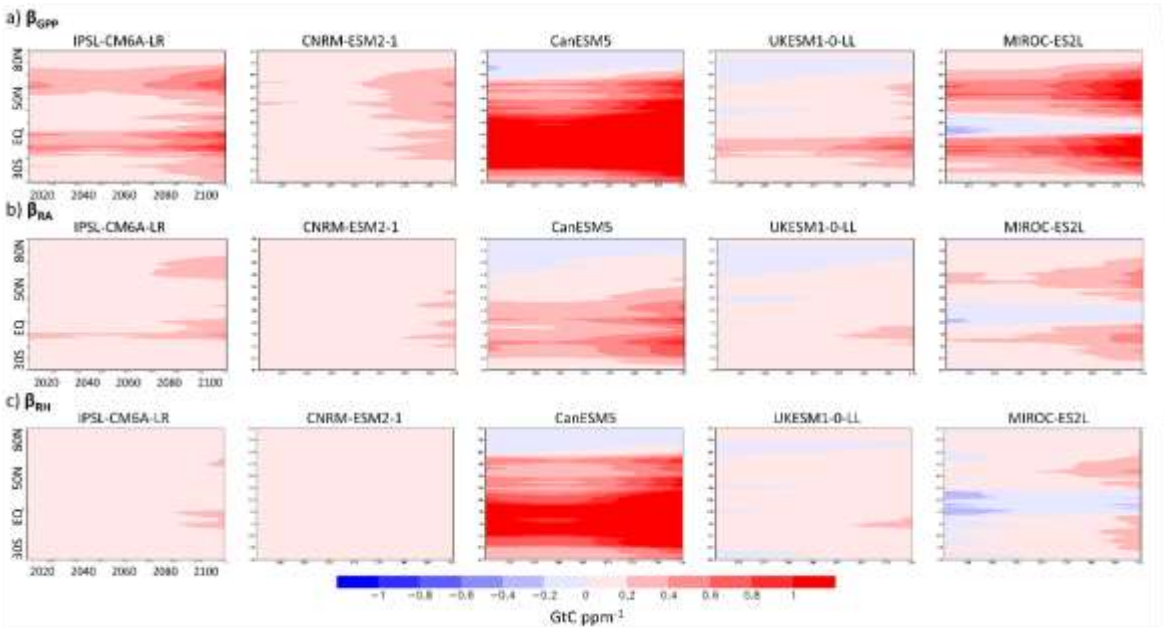

Figure S14. The spatiotemporal variation of zonal cumulative (a) β_{GPP}, (b) $\beta_{RA,}$ and (c) β_{RH} (GtC ppm^{-1}) is calculated from corresponding cumulative land carbon fluxes. Positive values indicate a net sink for β_{GPP} and a net source for β_{RA} and β_{RH}.

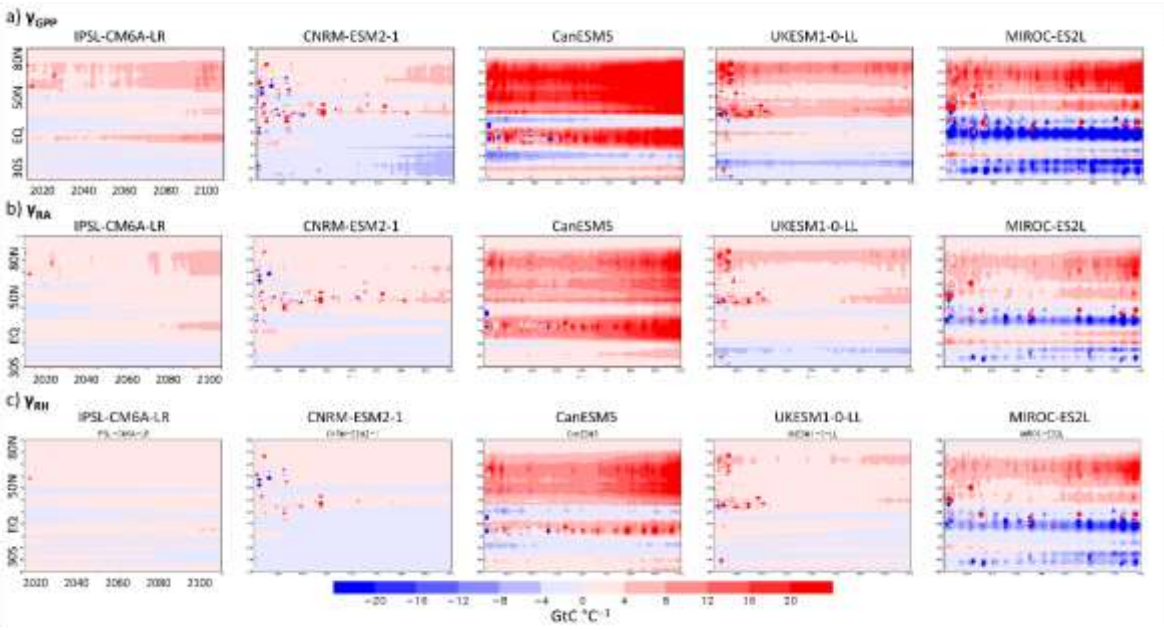

Figure S15. The spatiotemporal variation of zonal cumulative (a) γ_{GPP}, (b) γ_{RA}, and (c) γ_{RH} (GtC °C $^{-1}$) calculated from corresponding cumulative land carbon fluxes. Positive values indicate a net sink for γ_{GPP} and a net source for γ_{RA} and γ_{RH}.